Triple-vector-boson processes in $\gamma\gamma$ colliders

F. T. Brandt,[1] O. J. P. Éboli,[1] E. M. Gregores,[2] M. B. Magro,[1] P. G. Mercadante,[1], and S. F. Novaes[2]
[1]*Instituto de Física, Universidade de São Paulo, C.P. 20516, 01452-990 São Paulo, Brazil*
[2]*Instituto de Física Teórica, Universidade Estadual Paulista, Rua Pamplona 145, 0405-900 São Paulo, Brazil*
(Received 27 August 1993; revised manuscript received 23 March 1994)

We study the production of three gauge bosons ($W^+W^-Z^0$ and $W^+W^-\gamma$) at the next generation of linear e^+e^- colliders operating in the $\gamma\gamma$ mode. We analyze the total cross sections as well as several kinematical distributions of the final state particles. We find out that a linear e^+e^- machine operating in the $\gamma\gamma$ mode will produce 5–10 times more three-gauge-boson states compared to the standard e^+e^- mode at high energies.

PACS number(s): 12.15.Ji, 13.10.+q, 14.70.Fm, 14.70.Hp

I. INTRODUCTION

Nowadays, the possibility of transforming a linear e^+e^- collider into a $\gamma\gamma$ collider deserves a lot of attention. By using the old idea of Compton laser backscattering [1], it is possible to obtain very energetic photons from an electron or positron beam. The scattering of a laser with a few eV against an electron beam is capable of giving rise to a scattered photon beam carrying almost all the parent electron energy with a similar luminosity [2]. This mechanism can be employed in the next generation of e^+e^- linear colliders [3,4] [Next Linear Collider (NLC)] which will reach a center-of-mass energy of 500–2000 GeV with a luminosity of the order of 10^{33} $\mathrm{cm}^{-2}\,\mathrm{s}^{-1}$.

An important process that can take place at the NLC operating in the $\gamma\gamma$ mode is the production of vector-boson pairs through $\gamma\gamma \to W^+W^-$ [5], since this reaction has a very large cross section at high energies due to the W exchange in the t channel. Moreover, the available center-of-mass energy of the NLC will be large enough to produce final states presenting three-vector bosons with a significant event rate. Multiple-vector-boson production is very interesting for a number of reasons. First, the confirmation of the standard model predictions for the cross sections might provide further tests of the standard electroweak-gauge model. Second, the triple-gauge-boson production may be a background to possible signals from new physics beyond the standard model such as the production of invisibly decaying Higgs bosons in association with W^+W^- pairs [6]. Such Higgs bosons, presenting a large "invisible" branching ratio, appear in many extensions of the standard model that exhibit the spontaneous violation of a U(1) symmetry [7]. Third, the production of multiple-longitudinal-gauge bosons can shed light on the symmetry-breaking mechanism even when there is no contribution coming from the standard Higgs boson. For example, in models where the electroweak-symmetry-breaking sector is strongly interacting there is an enhancement of this channel [8,9].

In this work, we examine the production of three-vector bosons in $\gamma\gamma$ collisions through the reactions

$$\gamma + \gamma \to W^+ + W^- + Z^0 \,, \tag{I}$$

$$\gamma + \gamma \to W^+ + W^- + \gamma \,, \tag{II}$$

within the scope of the standard model. Previously, the cross sections for triple-gauge-boson production in this framework were presented for e^+e^- [10–12] and hadronic colliders [8,10]. We analyze the total cross section of these processes, as well as the kinematical distributions of the final-state vector bosons. We conclude that for a center-of-mass energy $\sqrt{s} \gtrsim 500$ GeV and an integrated luminosity of 10 fb^{-1}, there will be a promising number of fully reconstructible events even after discarding the unidentifiable W and Z decay channels. Moreover, we find out that a linear e^+e^- machine operating in the $\gamma\gamma$ mode will produce 5–10 times more three-gauge-boson states compared to the standard e^+e^- mode at high energies.

The outline of this paper is as follows. In Sec. II we introduce the laser backscattering spectrum, and present the details of the calculational method. Section III contains our results for the total cross section and the kinematical distributions of the final-state gauge bosons for center-of-mass energies $\sqrt{s} = 0.5$ and 1 TeV. In Sec. IV we discuss our results and compare them with some potential backgrounds. This paper is supplemented by an appendix which gives the invariant amplitudes for the above processes.

II. CALCULATIONAL METHOD

The cross section for the triple-vector-boson production via $\gamma\gamma$ fusion can be obtained by folding the elementary cross section for the subprocesses $\gamma\gamma \to WWV$ ($V = Z^0,\ \gamma$) with the photon luminosity ($dL_{\gamma\gamma}/dz$):

$$d\sigma(e^+e^- \to \gamma\gamma \to WWV)(s) = \int_{z_{\min}}^{z_{\max}} dz \frac{dL_{\gamma\gamma}}{dz} d\hat{\sigma}(\gamma\gamma \to WWV)\ (\hat{s} = z^2 s) \,, \tag{1}$$

 ©1994 The American Physical Society

where $\sqrt{s}$ ($\sqrt{\hat{s}}$) is the e^+e^- ($\gamma\gamma$) center-of-mass energy and $z^2 = \tau \equiv \hat{s}/s$. Assuming that the whole electron beam is converted into photons via the laser backscattering mechanism, the relation connecting the photon structure function $F_{\gamma/e}(x,\xi)$ to the photon luminosity is

$$\frac{dL_{\gamma\gamma}}{dz} = 2\,z \int_{z^2/x_{\max}}^{x_{\max}} \frac{dx}{x} F_{\gamma/e}(x,\xi) F_{\gamma/e}(z^2/x,\xi)\,. \quad (2)$$

For unpolarized beams the photon-distribution function [2] is given by

$$F_{\gamma/e}(x,\xi) \equiv \frac{1}{\sigma_C}\frac{d\sigma_c}{dx} = \frac{1}{D(\xi)}\left[1 - x + \frac{1}{1-x} - \frac{4x}{\xi(1-x)} + \frac{4x^2}{\xi^2(1-x)^2}\right], \quad (3)$$

with

$$D(\xi) = \left(1 - \frac{4}{\xi} - \frac{8}{\xi^2}\right)\ln(1+\xi) + \frac{1}{2} + \frac{8}{\xi} - \frac{1}{2(1+\xi)^2}\,, \quad (4)$$

where σ_C is the Compton cross section, $\xi \simeq 4E\omega_0/m_e^2$, m_e and E are the electron mass and energy, respectively, and ω_0 is the laser-photon energy. The fraction x represents the ratio between the scattered photon and initial electron energy for backscattered photons traveling along the initial electron direction. The maximum value of x is

$$x_{\max} = \frac{\omega_{\max}}{E} = \frac{\xi}{1+\xi}\,, \quad (5)$$

with $\omega_{\max}$ being the maximum scattered photon energy.

The fraction of photons with energy close to the maximum value grows with $\sqrt{s}$ and ω_0. Nevertheless, the bound $\xi < 2(1+\sqrt{2})$ should be respected in order to avoid the reduction in the efficiency of the $e \to \gamma$ conversion due to the creation of e^+e^- pairs in collisions of the laser with backscattered photons. We assumed that ω_0 has the maximum value compatible with the above constraint, e.g., for $\sqrt{s} = 500$ GeV, $\omega_0 = 1.26$ eV, and $x_{\max} \simeq 0.83$. With this choice, more than half of the scattered photons are emitted inside a small angle ($\theta < 5 \times 10^{-6}$ rad) and carry a large amount of the electron energy. Because of this hard photon spectrum, the luminosity Eq. (2) is almost constant for $z < x_{\max}$.

TABLE I. Total cross section in fb for the process $\gamma\gamma \to W^+W^-Z^0$.

$\sqrt{s}$ (GeV)	Without cuts	With cuts
500	20.4	10.2
1000	289	81.9

The analytical calculation of the cross section for the process $\gamma\gamma \to W^+W^-\gamma$ ($\gamma\gamma \to W^+W^-Z^0$) requires the evaluation of 12 Feynman diagrams in the unitary gauge, which is a tedious and lengthy calculation despite being straightforward. For the sake of completeness, we exhibit in the Appendix the expression of the amplitudes of these processes. In order to perform these calculations in an efficient and reliable way [13], we used an improved version of the numerical technique presented in Refs. [11,14]. The integrations were also performed numerically using a Monte Carlo routine [15] and we tested the Lorentz and $U(1)_{em}$ gauge invariances of our results for the amplitudes.

III. CROSS SECTIONS AND GAUGE-BOSON DISTRIBUTIONS

We have evaluated the total cross section for the processes $\gamma\gamma \to W^+W^-V$ imposing kinematical cuts on the final-state particles. Our first cut required that the produced gauge bosons are in the central region of the detector; i.e., we imposed that the angle of vector boson with the beam pipe is larger than 30°, which corresponds to a cut in the pseudorapidity of $|\eta| < 1.32$. We further required the isolation of the final particles by demanding that all vector bosons make an angle larger than 25° between themselves. Moreover, for the process II, we introduced a cut on the photon transverse momentum, $p_T^\gamma > 10$ GeV, to guarantee that the results are free of infrared divergences and to mimic the performance of a typical electromagnetic calorimeter.

In Tables I and II we exhibit the results for the total cross section of the processes I and II, with and without the above cuts. As we can see from these tables, the two-gauge-boson cross section ($\gamma + \gamma \to W^+ + W^-$), which is the main reaction in a $\gamma\gamma$ collider [5], is from 2 to 4 orders of magnitude above those for three-gauge bosons depend-

TABLE II. Total cross section in fb for the process $\gamma\gamma \to W^+W^-\gamma$.

	$P_T^\gamma > 10$ GeV		$P_T^\gamma > 20$ GeV	
$\sqrt{s}$ (GeV)	Without cuts	With cuts	Without cuts	With cuts
500	296	115	167	69
1000	1162	192	748	138

ing upon $\sqrt{s}$. Nevertheless, we still find promising event rates for final states W^+W^-V for an e^+e^- collider with an annual integrated luminosity of 10 fb^{-1}. Moreover, the triple-gauge-boson production in e^+e^- and $\gamma\gamma$ colliders are comparable at $\sqrt{s} = 500$ GeV, while the event rate in $\gamma\gamma$ collider is a factor of 5–10 larger than the one in an e^+e^- machine at $\sqrt{s} = 1$ TeV. The observed growth of the total cross section for the production of three-gauge bosons is due to gauge-boson exchange in the t and u channels.

Since we are interested in final states where all the gauge bosons are identified, the event rate is determined not only by the total cross section, but also by the reconstruction efficiency that depends on the particular decay channels of the vector bosons. In principle, charged lepton and light quark jet pairs can be easily identified. However, in the semileptonic decay of heavy quark the presence of unmeasurable neutrinos spoils the invariant mass measurement, and we adopt, as in Ref. [11], that the efficiency for reconstruction of a $W^{\pm}$ (Z^0) is 0.61 (0.65). In general, final-state photons can be identified with high efficiency as an electromagnetic shower with a neutral initiator. Combining the reconstruction efficiencies for individual particles, we obtain that the process I (II) has a detection efficiency of 0.24 (0.37). Once the reconstruction efficiency is substantial, the crucial factor for event rates is the production cross section. Assuming the above cuts and efficiencies we expect, for a 500 (1000) GeV collider with an annual integrated luminosity of 10 fb^{-1}, a total yield of 25 (198) $\gamma + \gamma \to W^+ + W^- + Z^0$ fully reconstructed events per year and 428 (714) $\gamma + \gamma \to W^+ + W^- + \gamma$ reconstructed events per year with $P_T^{\gamma} > 10$ GeV. It is instructive to compare these results with the number of fully recon-

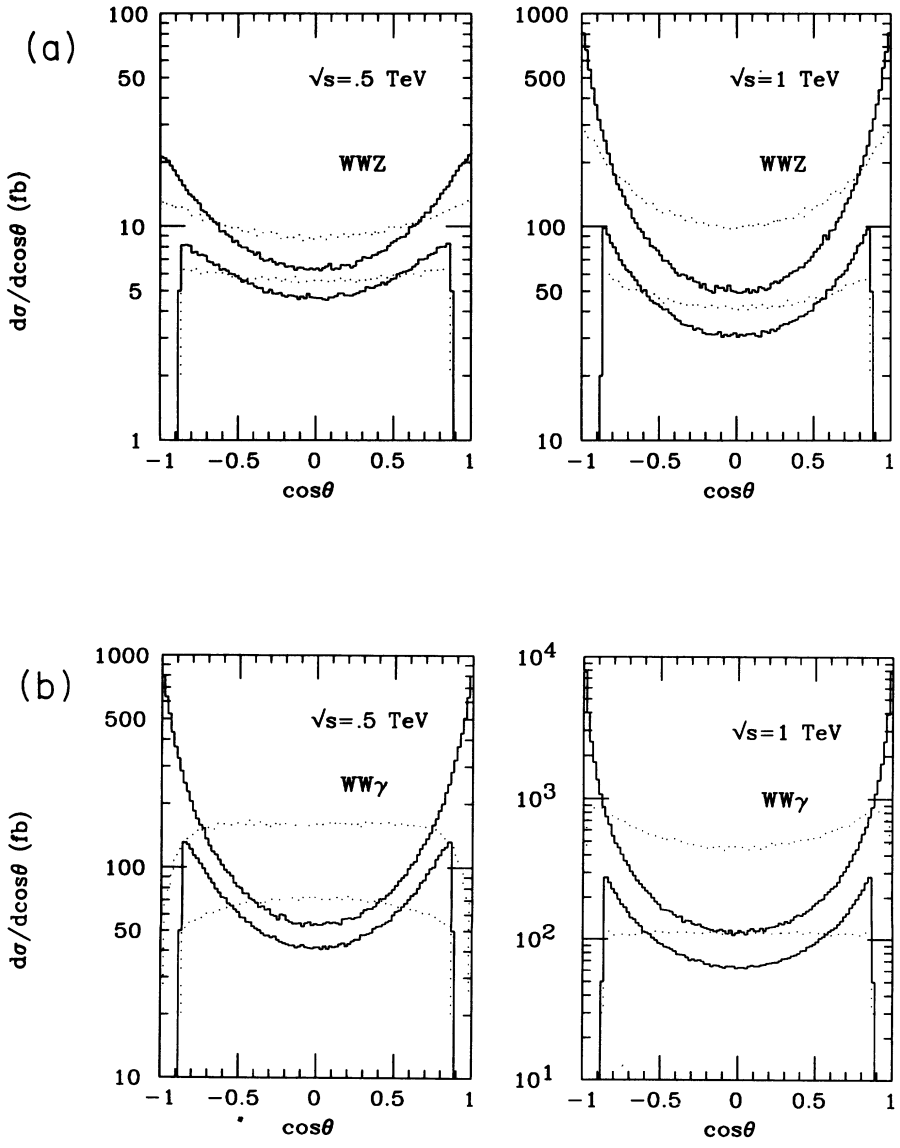

FIG. 1. Angular distributions of the vector bosons with the beam pipe. The upper (lower) solid lines stand for the W's, while the upper (lower) dashed line represents the V ($V = Z^0$ or γ) without (with) the cuts discussed in the text. For the $W^+W^-\gamma$ production we imposed the cut $p_T^{\gamma} > 10$ GeV.

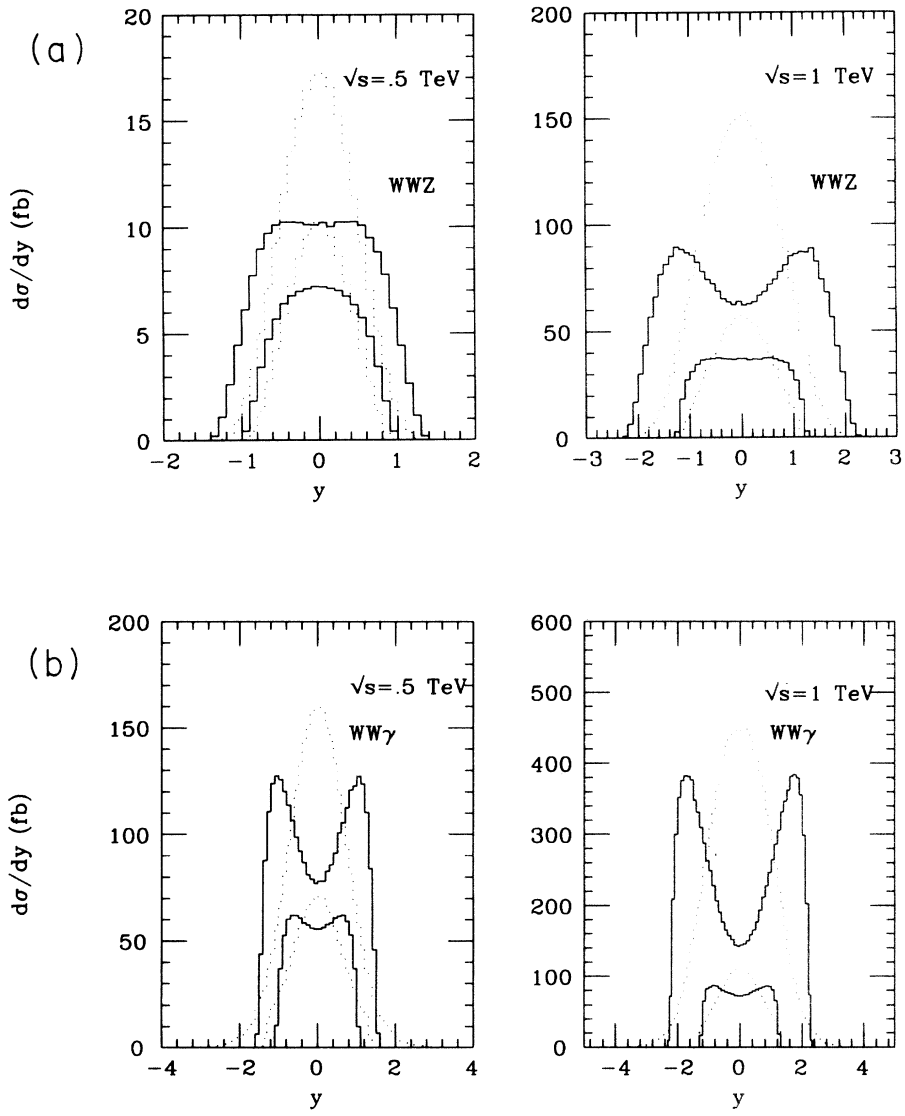

FIG. 2. Rapidity distributions. The conventions are the same as in Fig. 1.

structed events in $\gamma\gamma \to W^+W^-$. Employing the same reconstruction efficiency, angular cuts, and luminosity given above, there will be 9.4×10^4 (1.4×10^5) observed W^+W^- pairs for a center-of-mass energy of 500 (1000) GeV.

In order to reach a better understanding of reactions I and II, we present in Figs. 1–6 various distributions of the final-state gauge bosons. In Fig. 1 we show the distribution in $\cos\theta$, where θ is the polar angle of the particles ($W^{\pm}$, and $V = \gamma, Z^0$) with the beam pipe. The results are presented with and without the angular cuts described above. The W^+ and W^- curves coincide due to the charge-conjugation invariance. We should notice that these processes are particularly sensitive to central region requirement since, analogously to what happens in the reaction $\gamma\gamma \to W^+W^-$, the W's go preferentially along the beam pipe direction. This fact can also be seen from the rapidity distribution of the final-state particles (Fig. 2). Therefore, the requirement that the gauge bosons are produced in the central region of the detector implies in a loss of 1/2 to 5/6 of the total number of events. Increasing the center-of-mass energy, the W's tend to populate the high rapidity region while the $V = \gamma, Z^0$ distribution maintains its shape. Consequently, the cut in the W angle with beam pipe discards most of the high energy events.

In order to estimate the importance of the isolation cut on the final particles, we present in Fig. 3 the distributions in the angle between the vector bosons. Charge-conjugation invariance of the processes implies that the distributions for W^+Z^0 and W^-Z^0 are the same. In both processes I and II, the W's tend to be back to back, while the WV ($V = Z^0$ or γ) is relatively flat, demonstrating that the isolation cut is not very restrictive. The distribution for different energies of the collider are quite similar, apart from a constant factor due to the growth of the total cross section.

The invariant mass distributions of the W^+W^- and $W^{\pm}Z^0$ (γ) pairs are presented in Fig. 4. Once again the W^+Z^0 (γ) and W^-Z^0 (γ) curves coincide. From this

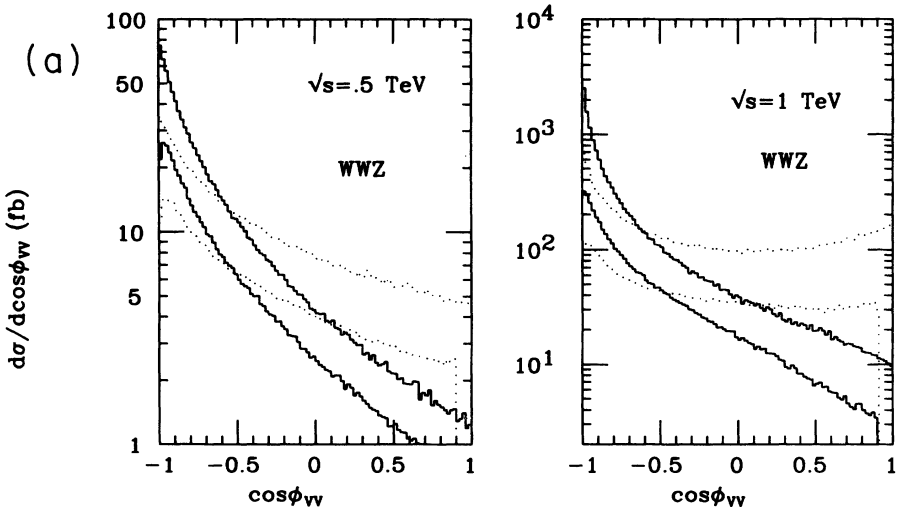

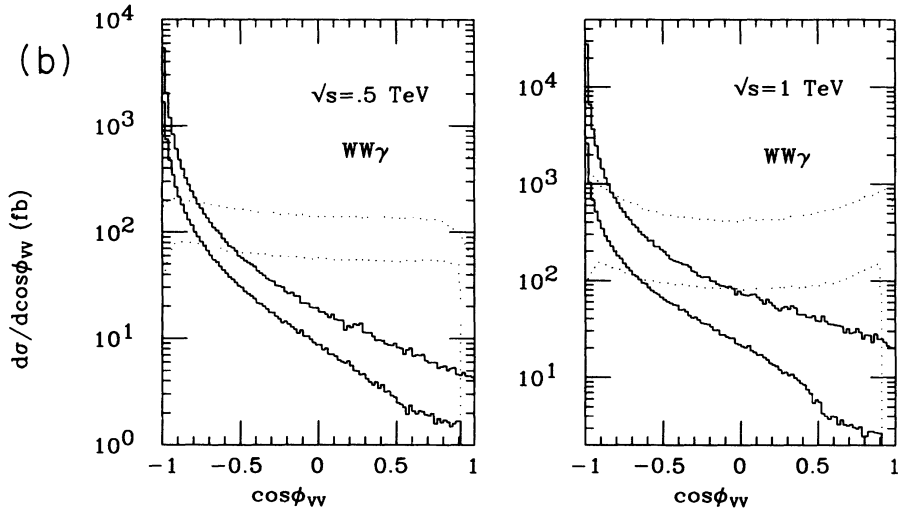

FIG. 3. Distributions of the angles between the pair of vector bosons. The upper (lower) solid line stands for the W^+W^- angle while the upper (lower) dashed line represents the WV angle without (with) the cuts discussed in the text. For the $W^+W^-\gamma$ production we imposed the cut $p_T^\gamma > 10$ GeV.

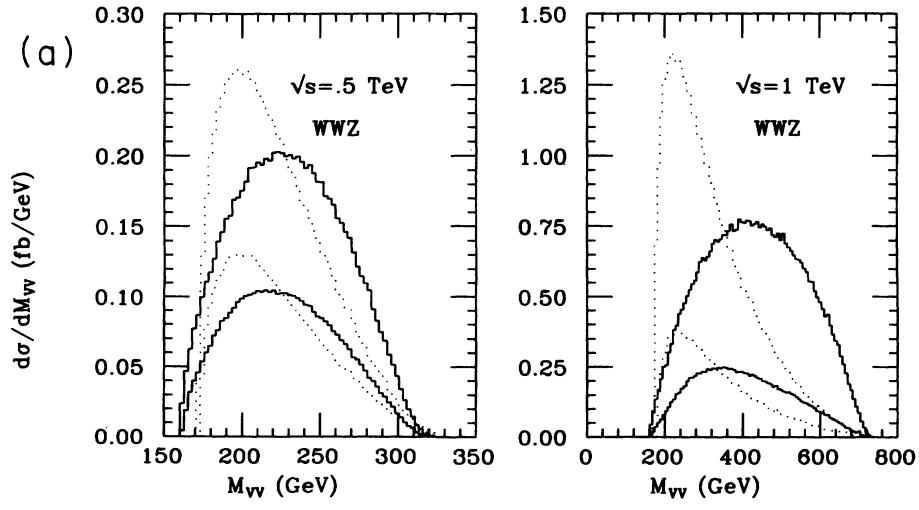

FIG. 4. Invariant-mass distributions. The conventions are the same as in Fig. 3.

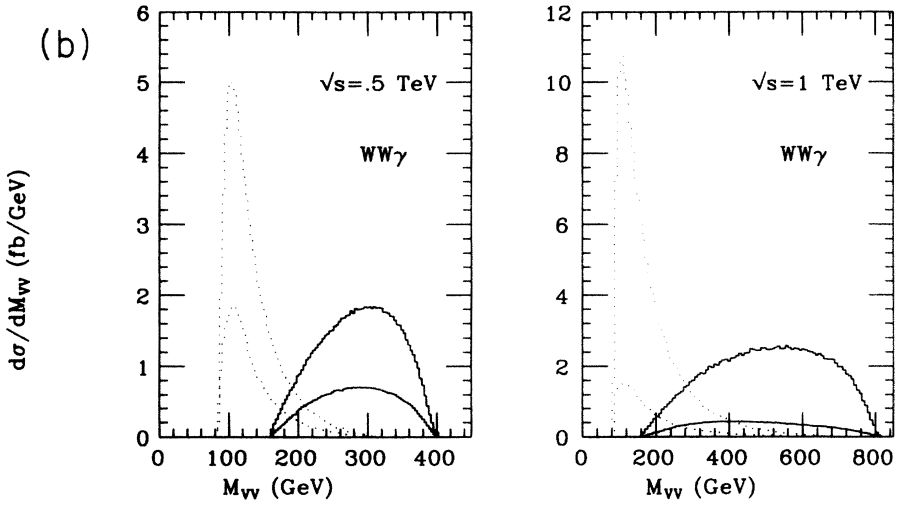

FIG. 4. (*Continued*).

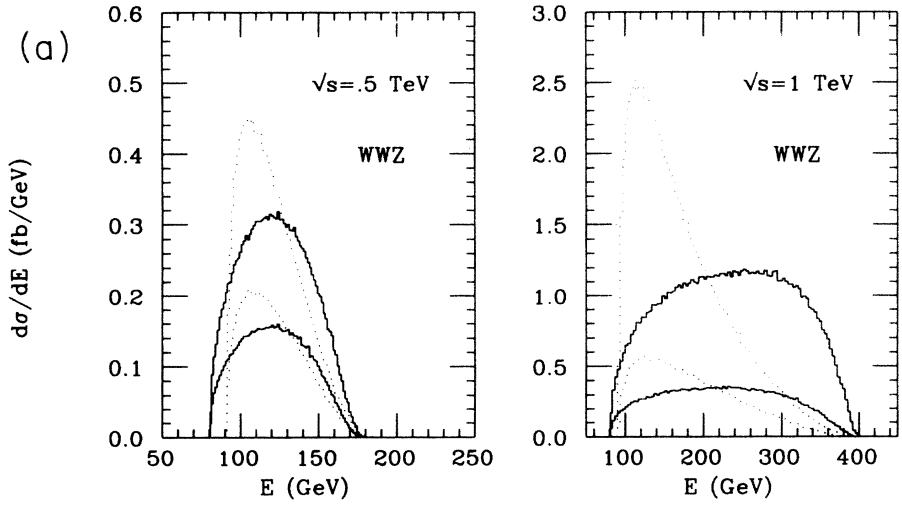

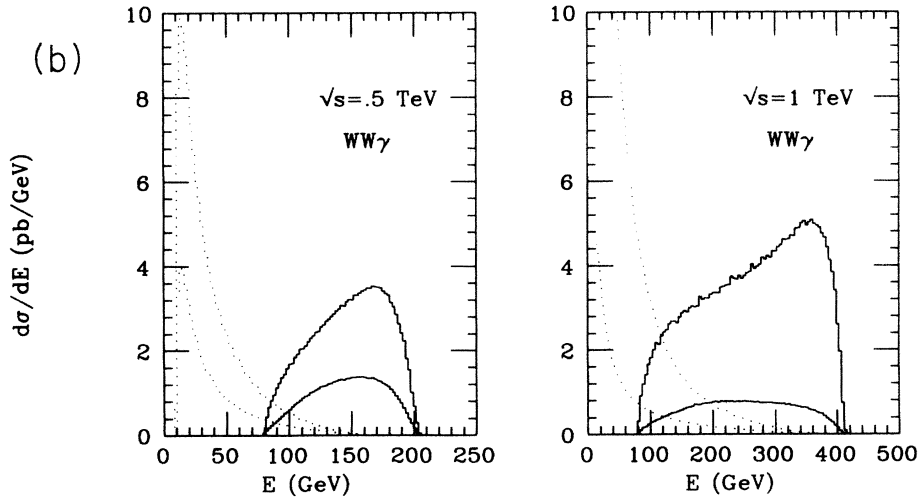

FIG. 5. Energy distributions. The conventions are the same as in Fig. 1.

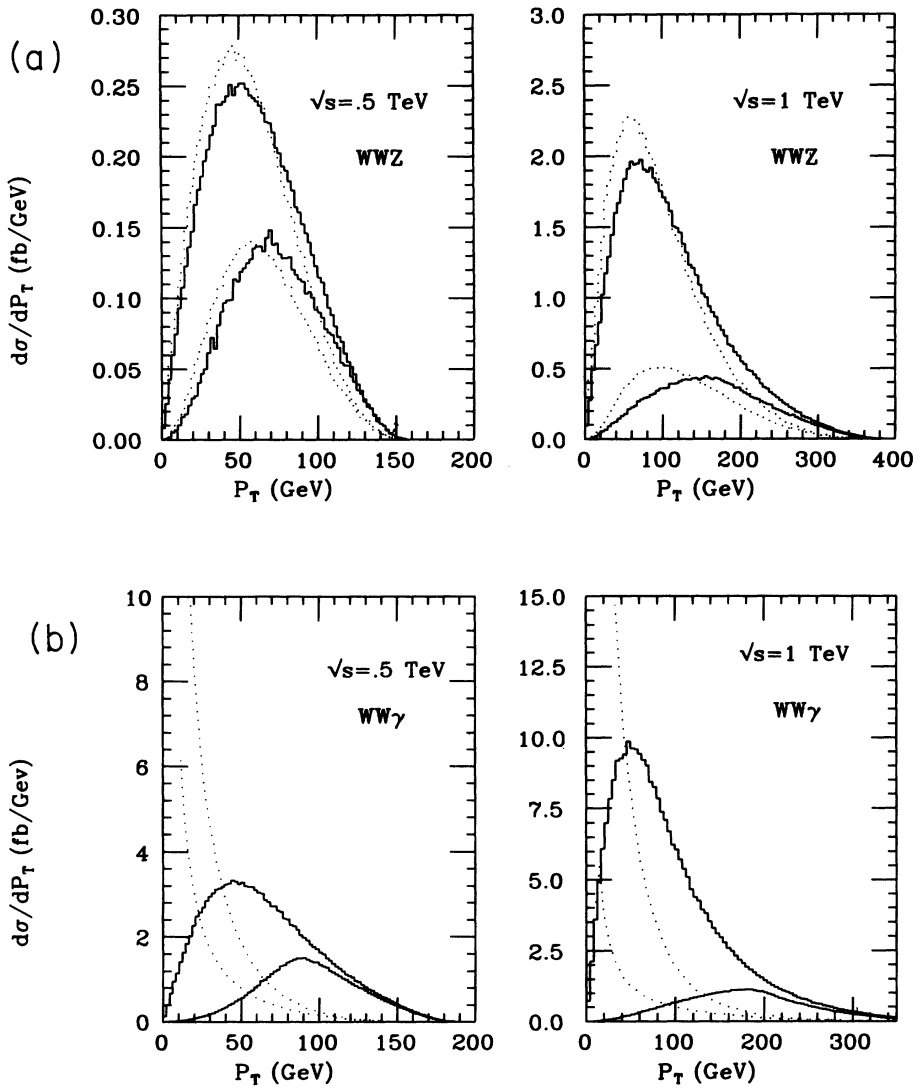

FIG. 6. Transverse momentum distributions. The conventions are the same as in Fig. 1.

figure we can learn that the average invariant mass of the pairs W^+W^- is higher than the one for WZ^0 (γ) pairs. As the center-of-mass energy of the collider is increased, the distributions grow due to the growth of the total cross section. Moreover, the invariant mass distributions for WZ^0 (γ) and W^+W^- pairs are considerably different: the former is rather narrow and peaked at small invariant masses while the latter one is broader and peaked at high invariant masses.

Figure 5 shows the laboratory energy distributions of the $W^\pm$ and Z^0 (γ) gauge bosons. In the process $\gamma\gamma \to W^+W^-Z^0$, the E_Z and $E_{W^\pm}$ distributions are rather similar, with the average energy of the $W^\pm$ being larger than the average Z^0 energy. As the center-of-mass energy of the collider increases, the distributions grow and become rather isolated, while the peaks broaden systematically. In the process $\gamma\gamma \to W^+W^-\gamma$, the distributions in E_γ and $E_{W^\pm}$ are very different due to the infrared divergences: the E_γ is strongly peaked towards small energies while $E_{W^\pm}$ is rather broad and peaked at high energies. With the increase of the collider energy the difference between these distributions becomes clearer.

We exhibit in Fig. 6 the transverse-momentum distribution for the $W^\pm$ and Z^0 (γ) vector bosons. There are no distinctive differences between the distribution for $W^\pm$ and Z^0 in process I, apart from the fact that the Z^0's exhibit a smaller average p_T than the W's. In the case of process II, the distributions for γ and $W^\pm$ are very different since the first is peaked at very small p_T due to the infrared divergences.

IV. DISCUSSION

The kinematical distributions presented in Figs. 1–6 were obtained by applying the angular cuts to the final-state vector bosons. Nevertheless, in order to have a more realistic description of the events, we should take into account the decay of the vector bosons since the final quarks can give rise to jets that either overlap or emerge

near the beam axis. To illustrate the changes in the total event rate and in the kinematical distributions when the cuts are applied to the W decay products, we evaluated the process

$$\gamma + \gamma \to [W^+ \to] q\bar{q}' + [W^- \to] q\bar{q}' + \gamma \,, \tag{6}$$

imposing the beam pipe cut $|\cos\theta| < 0.87$ and the isolation cut $\Delta R \equiv [(\Delta\eta)^2 + (\Delta\phi)^2]^{1/2} > 0.43$ among the final-state partons (quarks and photon). In addition, we also required a minimum transverse momentum of the photon of 10 (20) GeV.

The effect of applying the cuts to the decay products instead to the W's is to further reduce the total number of fully reconstructible events (6) by a factor $\simeq 0.6$, as can be seen from Table III. For instance, assuming the efficiencies and luminosity of Sec. III we expect, for a 500 (1000) GeV collider, 271 (444) reconstructed events with $P_T^\gamma > 10$ GeV, instead of the estimated 428 (714) events of the previous section. This reduction originates mainly from the fact that the isolation cut imposed on the W's does not guarantee that their decay products are isolated.

TABLE III. Total cross section in fb for the process $\gamma + \gamma \to [W^+ \to] q\bar{q}' + [W^- \to] q\bar{q}' + \gamma$ with cuts applied to the decay products of the W's. We have already taken into account the relevant branching ratios and reconstruction efficiencies as described in the text.

$\sqrt{s}$ (GeV)	$P_T^\gamma > 10$ GeV	$P_T^\gamma > 20$ GeV
500	27.1	16.8
1000	44.4	32.2

It is interesting to notice that the distributions 1–6 remain basically the same when we take into account the above partonic cuts, except for the P_T distribution of the

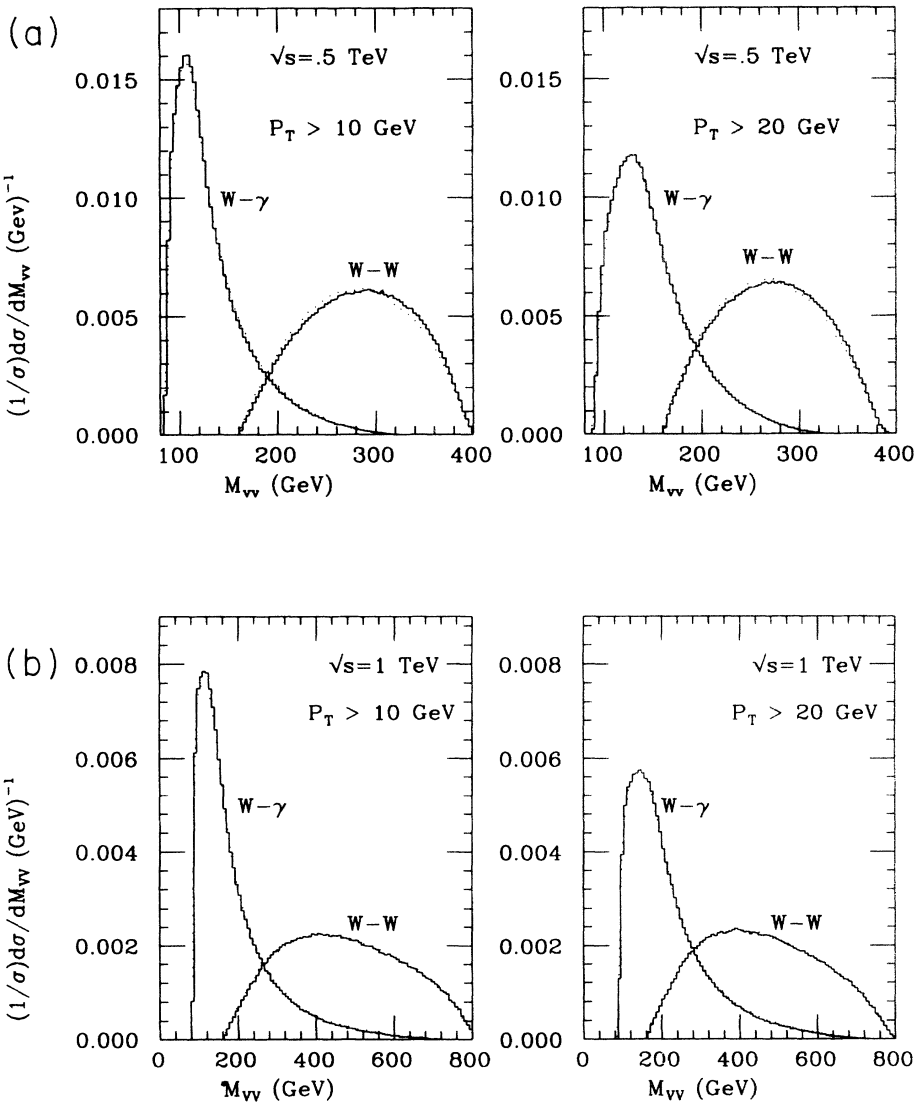

FIG. 7. Invariant-mass distributions of the WW and $W\gamma$ pairs with the cuts applied to the W's and γ (solid lines) and with the angular and isolation cuts (see text) imposed on the W decay products (dotted curves).

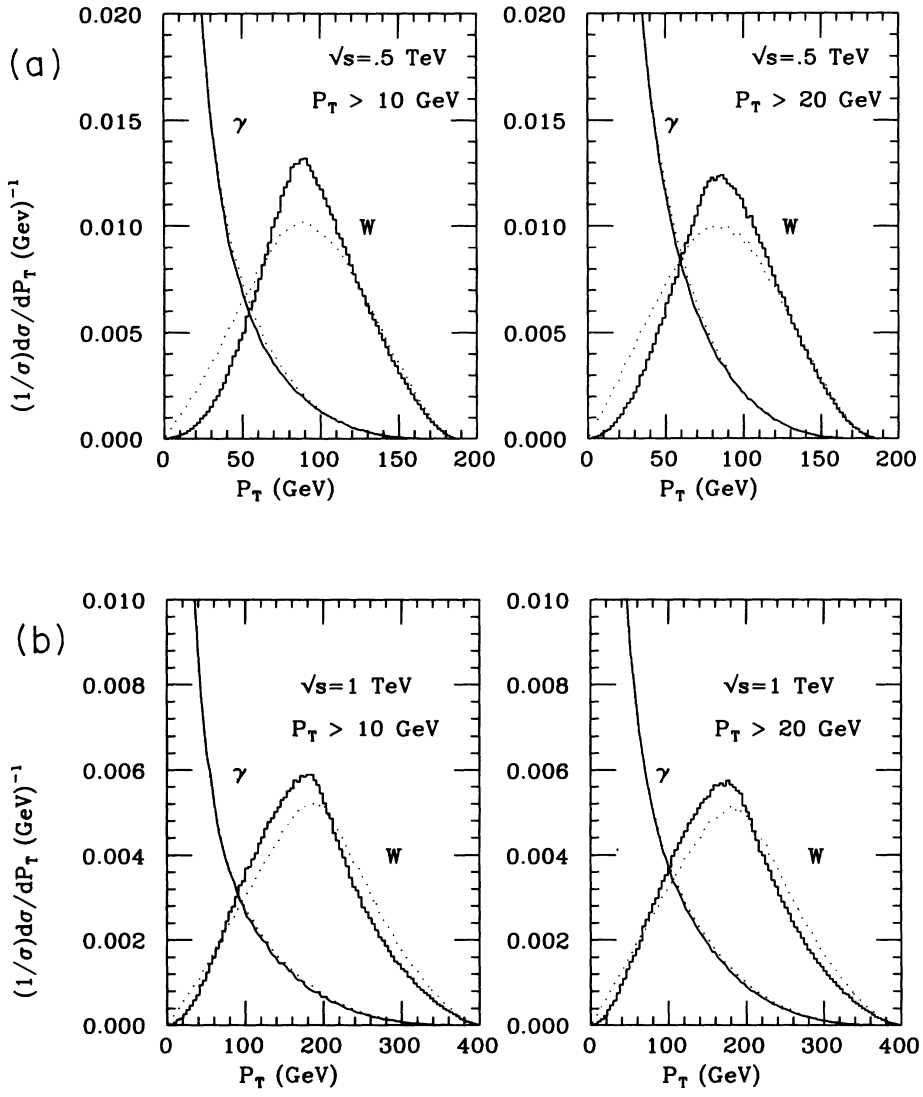

FIG. 8. Transverse momentum distributions of the W and γ. The conventions are the same as in Fig. 7.

W's that exhibits small qualitative changes. As an illustration, we present in Fig. 7 the normalized invariant mass distribution of WW and $W\gamma$ pairs with the cuts applied to the vector bosons and to their decay products, showing that the distributions have basically the same shape. On the other hand, we can see from Fig. 8 that the transverse momentum distribution of the W's presents a small increase in the fraction of events with small transverse momentum ($P_T < 40$ GeV), since the decay of some low-P_T W's can produce jets that do not necessarily emerge near the beam pipe even when the parent W is traveling in this direction.

At this point it is important to analyze other possible sources of $WW\gamma$ that could, at least in principle, be a background for the triple vector-boson production. For instance, the process $\gamma + \gamma \to W^+ + W^-$, which has a very large cross section, can lead to the same final state (6) when one of the on-shell W's decays into the three-body channel $W \to q\bar{q}'\gamma$, that is, the γ originates from bremsstrahlung of the decay products of the W [16]. A general feature of the bremsstrahlung process is that a large fraction of the events $W \to q\bar{q}'\gamma$ will have soft γ's that move preferentially in the q ($\bar{q}$) direction. Therefore, the above isolation and P_T^γ cuts are able to get rid

TABLE IV. Total cross section in fb for the background $\gamma + \gamma \to [W^+ \to]q\bar{q}' + [W^- \to]q\bar{q}' +$ "γ" with and without the cut in the invariant mass of the $q\bar{q}'$ pair. We have already taken into account the relevant branching ratios and reconstruction efficiencies as described in the text.

	$P_T^\gamma > 10$ GeV		$P_T^\gamma > 20$ GeV	
$\sqrt{s}$ (GeV)	Without $M_{q\bar{q}'}$ cut	With $M_{q\bar{q}'}$ cut	Without $M_{q\bar{q}'}$ cut	With $M_{q\bar{q}'}$ cut
500	11.8	1.55	5.92	0.263
1000	5.55	0.777	3.00	0.122

of a large amount of these events with bremsstrahlung photons.

We can improve our signal over background ratio even more by demanding that the final state exhibits two pairs of jets with an invariant mass compatible with the W mass. This requirement must reduce the rate of bremsstrahlung events since the jet–jet invariant mass of these events usually deviates from the value of the W mass. Taking into account the performance of a typical detector for the NLC, we required, among all the four final-state jets, the existence of two jet pairs with $|M_{jj} - M_W| \leq 10$ GeV. In Table IV we show the total cross section for the background reaction $\gamma + \gamma \to [W^+ \to]q\bar{q}' + [W^- \to]q\bar{q}' +$ "γ", where "γ" denotes the photon coming from the real $W^\pm$ fragmentation, when we apply this invariant mass cut. We present our results for two different values of the cut in P_T^γ (10 and 20 GeV) with the same isolation and beam pipe cuts described above, taking into account the relevant branching ratios and reconstruction efficiencies. This invariant mass cut eliminates approximately 90% of the background events. On the other hand, the invariant mass of the jet pairs coming from the signal $WW\gamma$ is peaked at M_W and is insensitive to this cut. In this way, we were able to improve the signal over background ratio 1–2 orders of magnitude depending on the center-of-mass energy and the P_T^γ cuts (see Table IV).

Note added in proof. After completing this paper we came across an estimate for the elementary cross section of the processes studied here [17]. We verified that our results before cuts and decays agree with the ones presented in Ref. [17].

ACKNOWLEDGMENTS

This work was partially supported by Conselho Nacional de Desenvolvimento Científico e Tecnológico (CNPq), and by Fundação de Amparo à Pesquisa do Estado de São Paulo (FAPESP).

APPENDIX

We collect in this appendix the expressions for the amplitudes of the processes $\gamma\gamma \to W^+W^-V$, with $V = Z^0$ or γ. The Feynman diagrams contributing to these processes are given in Fig. 9. The momenta and polarizations of the initial photons were denoted by (k_1, k_2) and $(\epsilon_\mu(k_1), \epsilon_\nu(k_2))$, while the momenta and polarizations of the final state W^+, W^-, and V are given by (p_+, p_-, k_3) and $(\epsilon_\alpha(p_+), \epsilon_\beta(p_-), \epsilon_\gamma(k_3))$, respectively. For a given choice of the initial and final polarizations the amplitude of these processes can be written as

$$M = G_v \epsilon_\mu(k_1)\epsilon_\nu(k_2)\epsilon_\alpha(p_+)\epsilon_\beta(p_-)\epsilon_\gamma(k_3) M_T^{\mu\nu\alpha\beta\gamma} , \quad \text{(A1)}$$

with

$$M_T^{\mu\nu\alpha\beta\gamma} = \sum_{i=1}^{7} M_i^{\mu\nu\alpha\beta\gamma} , \quad \text{(A2)}$$

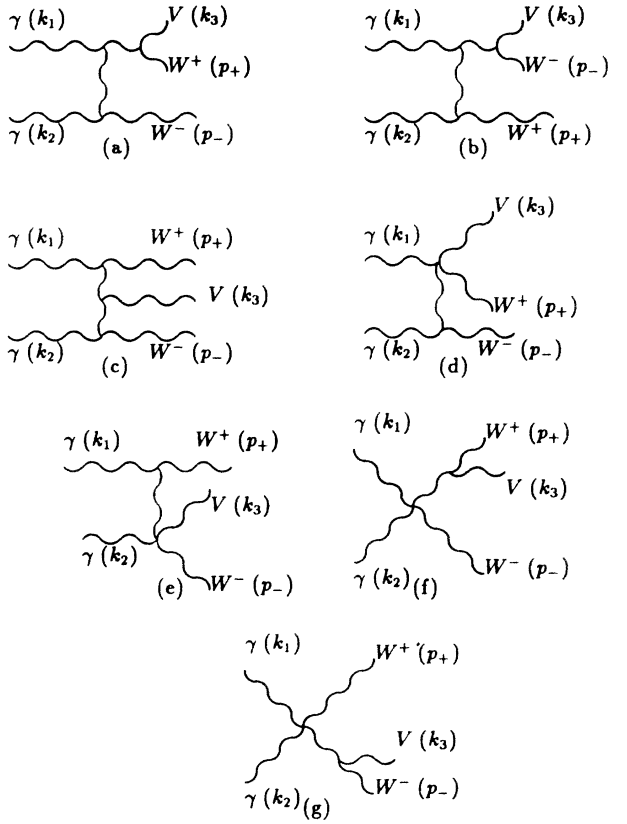

FIG. 9. Feynman diagrams that contribute to the process $\gamma\gamma \to W^+W^-V$ with $V = Z^0$ or γ.

where the $M_i^{\mu\nu\alpha\beta\gamma}$ is the contribution of the set of diagrams i to the processes. The factor G_v depends upon the process, assuming the value e^3 for the production of $W^+W^-\gamma$ and the value $e^3 \cot^2\theta_W$, with θ_W being the Weinberg angle, for the final state $W^+W^-Z^0$.

In order to write a compact expression for the amplitude, it is convenient to define the triple-gauge-boson coupling coefficient as

$$\Gamma_3^{\alpha\beta\gamma}(P_1, P_2) = [(2P_1 + P_2)^\beta g^{\alpha\gamma} - (2P_2 + P_1)^\alpha g^{\beta\gamma} + (P_2 - P_1)^\gamma g^{\beta\alpha}] , \quad \text{(A3)}$$

the quartic-gauge-boson coupling

$$\Gamma_4^{\mu\nu\alpha\beta} = g^{\mu\alpha}g^{\nu\beta} + g^{\mu\beta}g^{\nu\alpha} - 2g^{\mu\nu}g^{\alpha\beta} , \quad \text{(A4)}$$

and the propagator tensor

$$D^{\mu\nu}(k) = \frac{(g^{\mu\nu} - k^\mu k^\nu/m^2)}{k^2 - m^2} . \quad \text{(A5)}$$

Using the above definitions, the contributions of the different set of diagrams can be written as

$$M_1^{\mu\nu\alpha\beta\gamma} = \Gamma_3^{\alpha\gamma\xi}(p_+,k_3)D_{\xi\sigma}(p_+ + k_3)\Gamma_3^{\mu\sigma\rho}(k_1,-(p_+ + k_3))D_{\rho\lambda}(p_- - k_2)\Gamma_3^{\beta\nu\lambda}(-p_-,k_2) + [k_{1\leftrightarrow 2}\ ;\ \mu \leftrightarrow \nu], \quad \text{(A6)}$$

$$M_2^{\mu\nu\alpha\beta\gamma} = \Gamma_3^{\alpha\beta\xi}(k_3,p_-)D_{\xi\sigma}(p_- + k_3)\Gamma_3^{\sigma\nu\rho}(-p_- - k_3,k_2)D_{\rho\lambda}(k_1 - p_+)\Gamma_3^{\mu\alpha\lambda}(-p_+,k_2) + [k_{1\leftrightarrow 2}\ ;\ \mu \leftrightarrow \nu], \quad \text{(A7)}$$

$$M_3^{\mu\nu\alpha\beta\gamma} = \Gamma_3^{\mu\alpha\xi}(k_1,-p_+)D_{\xi\sigma}(k_1 - p_+)\Gamma_3^{\gamma\sigma\rho}(-k_3,(k_1 - p_+))D_{\rho\lambda}(p_- - k_2)\Gamma_3^{\nu\beta\lambda}(-k_2,p_-) + [k_{1\leftrightarrow 2}\ ;\ \mu \leftrightarrow \nu], \quad \text{(A8)}$$

$$M_4^{\mu\nu\alpha\beta\gamma} = \Gamma_3^{\beta\nu\xi}(-p_-,k_2)D_{\xi\lambda}(k_2 - p_-)\Gamma_4^{\lambda\alpha\mu\gamma} + [k_{1\leftrightarrow 2}\ ;\ \mu \leftrightarrow \nu], \quad \text{(A9)}$$

$$M_5^{\mu\nu\alpha\beta\gamma} = \Gamma_3^{\mu\alpha\xi}(k_1,-p_+)D_{\xi\lambda}(k_1 - p_+)\Gamma_4^{\lambda\beta\nu\gamma} + [k_{1\leftrightarrow 2}\ ;\ \mu \leftrightarrow \nu], \quad \text{(A10)}$$

$$M_6^{\mu\nu\alpha\beta\gamma} = \Gamma_3^{\alpha\gamma\xi}(p_+,k_3)D_{\xi\lambda}(p_+ + k_3)\Gamma_4^{\lambda\beta\nu\mu}, \quad \text{(A11)}$$

$$M_7^{\mu\nu\alpha\beta\gamma} = \Gamma_3^{\gamma\beta\xi}(k_3,p_-)D_{\xi\lambda}(-p_- - k_3)\Gamma_4^{\lambda\alpha\nu\mu}, \quad \text{(A12)}$$

where $[k_{1\leftrightarrow 2}\ ;\ \mu \leftrightarrow \nu]$ indicates the crossed contributions of the initial photons.

[1] F. R. Arutyunian and V. A. Tumanian, Phys. Lett. **4**, 176 (1963); R. H. Milburn, Phys. Rev. Lett. **10**, 75 (1963); see also C. Akerlof, University of Michigan Report No. UMHE 81-59, 1981 (unpublished).

[2] I. F. Ginzburg, G. L. Kotkin, V. G. Serbo, and V. I. Telnov, Nucl. Instrum. Methods **205**, 47 (1983); **219**, 5 (1984); V. I. Telnov, *ibid.* **A294**, 72 (1990).

[3] R. B. Palmer, Annu. Rev. Nucl. Part. Sci. **40**, 529 (1990).

[4] D. L. Burke, in *Proceedings of the XXVI International Conference on High Energy Physics*, Dallas, Texas 1992, edited by J. Sanford, AIP Conf. Proc. No. 272 (AIP, New York, 1993).

[5] I. F. Ginzburg, G. L. Kotkin, S. L. Panfil, and V. G. Serbo, Nucl. Phys. **B228**, 285 (1983).

[6] A. Lopez-Fernandez, J. C. Romão, F. de Campos, and J. W. F. Valle, Phys. Lett. B **312**, 240 (1993); O. J. P. Éboli, M. C. Gonzalez-Garcia, A. Lopez-Fernandez, S. F. Novaes, and J. W. F. Valle, Nucl. Phys. **B421**, 65 (1994).

[7] R. Barbieri and L. Hall, Nucl. Phys. **B364**, 27 (1991); J. C. Romão, F. de Campos, and J. W. F. Valle, Phys. Lett. B **292**, 329 (1992); A. Joshipura and J. W. F. Valle, Nucl. Phys. **B397**, 105 (1993).

[8] M. Golden and S. Sharpe, Nucl. Phys. **B261**, 217 (1985).

[9] M. Chanowitz and M.K. Gaillard, Phys. Lett. **142B**, 85 (1984).

[10] V. Barger and T. Han, Phys. Lett. B **212**, 117 (1988).

[11] V. Barger, T. Han, and R. J. N. Phillips, Phys. Rev. D **39**, 146 (1989).

[12] A. Tofighi-Niaki and J. F. Gunion, Phys. Rev. D **39**, 720 (1989).

[13] We have also checked our results using the analytical amplitudes obtained using REDUCE and FORM. It turned out that the numerical evaluation of cross sections and distributions by the numerical technique is at least ten times faster than the analytical results obtained with REDUCE and FORM.

[14] K. Hagiwara and D. Zeppenfeld, Nucl. Phys. **B274**, 1 (1986).

[15] G. P. Lepage, J. Comput. Phys. **27**, 192 (1978).

[16] J. Ohnemus and W. J. Stirling, Phys. Rev. D **47**, 336 (1993).

[17] M. Baillargeon and F. Boudjema, in *Beyond of the Standard Model III*, Procededings of the Workshop, Ottawa, Ontario, 1992, edited by S. Godfrey (World Scientific, Singapore, 1993); Phys. Lett. B **317**, 371 (1993).